JOURNAL OF COMPUTATIONAL PHYSICS 118, 278–293 (1995)

A Method for Near Field Computation of Coupled Weakly Ionized Plasma Flows in Low Earth Orbit

CHARLES R. JUSTIZ AND RONALD M. SEGA

National Aeronautics and Space Administration, Lyndon B. Johnson Space Center, Houston, Texas 77058

AND

CHARLES DALTON

Mechanical Engineering Department, University of Houston, Houston, Texas 77204-4814

Received October 4, 1994

The problem of wake effects, particularly the near wake, from spacecraft in low Earth orbit is of increasing interest. The flow simulation reported herein combines the fully coupled effects of neutral particle flow, plasma flow, electromagnetic field effects, and spacecraft charging. The simulation necessarily allows for chemically reacting flows (associative ionization, dissociation, and chain exchange) and for thermal accommodation at a spacecraft surface. Due to the highly coupled nature of the flow physics, a full solution simultaneous approach is used. This is required due to the need for extremely high resolution results for the near wake region. In this approach, the neutral flow is modeled using a direct simulation Monte Carlo technique. The charged particles are modeled using a particle approach to solve the Poisson equation. A technique of having a separate neutral-particle grid and a charged-particle grid is used. Neutral and charged particles are allowed collisional interaction. During one time step, the neutral-particle-move process occurs separately from the charged-particle-move process which is accomplished in the presence of the electromagnetic field. A major advantage of the technique is that results may be obtained with the dominant effects of orbital flows simultaneously modeled. A major disadvantage is that the technique is computationally expensive. Flow calculations for the neutral- and charged-particle cases are compared to independent and uncoupled computational simulations to confirm their accuracy. The solution procedure and technique are presented for several types of flows at orbital altitudes of 250 and 500 km. Excellent agreement with previously verified computational algorithms has been obtained for the case of neutral particle flow and charged-particle flow. Results for the full flow simulation are presented for 250 and 500 km.

1. INTRODUCTION

Contamination and space-environment effects of a spacecraft in low Earth orbit (LEO) (200 to 600 km) have attracted a great deal of attention recently. Current examples of programs in the United States that concern high-resolution coupled-flow determinations are the operations of the Space Station Freedom (NASA, 1986), retrieval of on-orbit test equipment such as the Long Duration Exposure Facility (LDEF) (Kinard, 1991), and the epitaxial thin film experiment using the Wake Shield Facility (WSF) (Sega and Ignatiev, 1991). Contamination and environmental effects are also of great interest to the Russian Space Agency with respect to their space station *MIR's* docking contamination effects as well as open system contamination effects.

The primary objective of this investigation is to develop the capability to calculate the full flow of the near field environment of a weakly ionized, rarefied gas medium of which a specific case is a spacecraft in LEO. Due to the nature of the environment, the simulation includes the highly coupled effects of neutral particle flow, free stream plasma flow, nonequilibrium gas dynamics effects, spacecraft charging and electromagnetic field effects. Previous attempts have incompletely modeled the plasma flow physics and have not been able to include the field effects in the flow. The plasma flow physics are required due to the need for extremely detailed flow information in the near wake region. Our model can be applied to the prediction of vacuum levels to be generated by the WSF and developed for application to space station conditions as well as for other spacecraft. The WSF is a metallic disk-type structure (12 feet in diameter) that provides a good starting point for modeling.

For the purposes of this investigation, the WSF was computationally modeled as a 12-foot diameter disk with no thickness. The calculations presented herein are axisymmetric while the code developed was three dimensional. The results of this study are preliminary to forthcoming three-dimensional results using the full capability of the code.

The method of investigation proposed is a direct simulation of the flow field using the actual atmospheric conditions as described in *U.S. Standard Atmosphere* (N.O.A.A., 1976) and *International Reference Ionosphere* (Rawer, 1981). The simulation is done on a Class 6 computer using a hybrid method of direct numerical solution of the Maxwell equations (DNSME) with a direct simulation Monte Carlo (DSMC) method. The

0021-9991/95 $6.00

DNSME is used to resolve the flow characteristics due to electromagnetic effects, while the DSMC method is used to resolve the molecular collision dynamics on the sub-grid scale.

2. COMPUTATIONAL INVESTIGATION

The flexibility required for the investigation plus the difficulties with direct numerical solutions of the governing equations suggested a direct computer simulation of the motion of the atomic particles. Even using the extremely powerful capabilities of the National Aeronautics and Space Administration's (NASA) Numerical Aerodynamic Simulator (NAS), a probabilistic approach for the molecular collisional dynamics was required. Other kinetic properties did not require a probabilistic approach and were directly simulated.

Several assumptions were required to make the problem tractable for the initial investigations:

—A variable hard sphere (VHS) molecular model (e.g., Bird, 1978; Justiz and Sega, 1991) was used to simulate the particle collisional cross section. The function of the variation of the molecular diameter with relative velocity is to reproduce the viscosity–temperature behavior of real gases. It has been combined with phenomenological models for internal modes that can allow for partially excited modes and, therefore, a variable specific heat ratio. A simplification to the VHS model was used for this work which was similar to an assumption of a constant ratio of specific heats.

—Only binary collisions are allowed and collisions are "perfectly" elastic or "perfectly" inelastic. In this context, the term "perfectly" implies that all particles represented by the weighted binary collision pair will undergo the same elastic or inelastic collision process. While this is not physically correct, it is statistically correct.

—The earth's magnetic field is assumed to have a negligible effect on the process and was not included in the primary investigation.

—Only coulombic interaction is allowed between two charged particles. Collisions between an ion and a neutral particle are allowed.

—The plasma is pseudo-electrostatic.

—Postcollision parameters are distributed according to the Larsen–Borgnakke method. The equilibrium distributions that are employed in the derivation of this method have an effective temperature that is based on the collision energy and it varies with each collision. The distribution of the collision energy properly reflects the nonequilibrium that may exist in the gas provided that the collision time step is sufficiently small with respect to the collisional processes during a given time step in a given cell.

—The computational geometry is three dimensional with no simplifications with respect to symmetry. As the CARLOS code (see below) was developed to investigate asymmetric plasma flows, no two-dimensional or axisymmetric version was developed.

A series of programs was developed to model the flow of charged particles about a space structure. These were designated by the CARLO prefix to indicate that this was a direct simulation Monte Carlo method and by a suffix of S for a sequential machine, V for a vector machine, or P for a parallel machine. Herein, the term CARLOS will be used to describe the program regardless of the computer in which a specific data set was run. All program algorithms are identical except for the architecture-specific optimization. As all of the flow properties required from the study are of a macroscopic nature, the appropriate numerical solution method appears to be a DSMC. The DSMC method differs from other computational rarefied gas dynamics (CRGD) techniques in that it statistically simulates the intermolecular kinetics and chemistry without directly solving the kinetic equations or governing equations at any stage. In DSMC, the kinetic equations are the basis of a statistical simulation model or, equivalently, direct experimental results are the basis for the statistical simulation model.

An overview of the method follows:

—Generate an appropriate grid space which represents physical space and is fixed to the frame of reference of interest. For statistical considerations, the grid generated is initialized such that approximately 20 to 30 particles are in each cell.

—Two time scales are used. The continuous real time τ is replaced by a discrete time step $\Delta\tau$ and a cell time counter $\Delta\tau_c$ is introduced.

—The flow is initialized with an appropriate number of particles (10^6) where each particle is characterized by its velocity vector, position vector, internal energy state, charge, and species. Also, the initial electromagnetic field is established.

—At each discrete time step $\Delta\tau$, each one of the cells is examined and the choice of collision partners and collisions are statistically simulated. At this point, only the velocities of the particles are changed.

—The particle-move process is broken into two separate sections, the neutral-particle-move process and the charged-particle-move process. In the charged-particle-move process, computation on neutral particles is stopped and a second grid structure, the charged-particle grid structure, is used. The charged-particle move is then accomplished on the new grid structure until the charged-particle clock has synchronized with the neutral-particle clock. Interactions with boundaries and surfaces are tested for and handled during each particle move. The charged particles are then reinserted into the spatial grid. The neutral particles are then moved to their next appropriate cells or to appropriate interactions with boundaries and surfaces. The sizes of these two grid systems will be cited later.

2.1. *Neutral Particle Simulation Method*

Several gas–surface interaction models can be employed. This study uses a modified model which was designed to corre-

late with recent low energy atomic oxygen studies such as that of Knox *et al.* (1991). Tangential and perpendicular thermal accommodation modeling is tailored to match that of Knox *et al.* Runs to be described later were made to verify the gas–surface interaction. Due to several differences in the molecular model over the standard DSMC model, performance in several areas was improved. Specifically, it is generally recognized that many models used in DSMC codes do not satisfy reciprocity or detailed balance. Elimination of the cloning technique has allowed several modifications which improve the performance in these areas. Unfortunately, the data for low energy atomic oxygen gas–surface interaction are not conclusive. This issue remains as a major problem for modeling orbital flows. Collisions involving neutrals are modeled using a VHS method (Bird, 1976). In other words, if σ_{ab} is the total collision cross section for collisions between species a and species b, then we have

$$\sigma_{ab}=\left[\frac{1}{2}\left\{\sigma_{aa}\left(\frac{m_a c_r^2}{4}\right)^{\omega}\right\}_{\text{ref}}^{1/2}+\frac{1}{2}\left\{\sigma_{bb}\left(\frac{m_b c_r^2}{4}\right)^{\omega}\right\}_{\text{ref}}^{1/2}\right]^2 E_c^{-\omega}, \quad (1)$$

where c_r is the relative speed between the two particles, m_a and m_b are the respective masses, E_c is the collision energy, ω is a simplification of the exponent of distance of an inverse power intermolecular force law relation, η, and is given by

$$\omega=\frac{2}{\eta-1}. \quad (2)$$

The actual number of molecules in a given flow situation cannot be modeled on present day computers. Consequently, simulated molecules involving weighting factors must be used. Thus, the weighting factor, W_a, for species a is

$$W_a=X_a\frac{n_\infty V_{\text{TOT}}}{n_{\text{sim}}}, \quad (3)$$

where n_∞ is the free stream number density, X_a is the free stream mole fraction of species a, V_{TOT} is the total computational volume, and n_{sim} is the number of particles in the simulation. Thus, the total number density n_j in a given cell j can be found for N_s number of species from

$$n_j=\sum_{i=1}^{N_s}\frac{n_i W_i}{V_j}, \quad (4)$$

where V_j is the cell volume of cell j and the index i is the species index for species a, b, ..., N_s. We use the classical elastic collision mechanics and collision energy descriptions as represented by Bird (1976). Inelastic collisions are described in the same manner except that the internal degrees of freedom of each particle are taken into account. A major difference from classical DSMC techniques is the elimination of molecular removal and duplication associated with radial weighting factors (cloning) through the use of advanced data structures. This was considered necessary due to the need to preserve molecular information in the near wake region, especially in the regions of rapid expansion.

2.2. *Charged Particle Simulation Method*

Various properties of the space environment allow simplifying assumptions to be made concerning the plasma environment:

—The plasma is pseudo-collisionless—the motion of the charged particles is dominated by the electromagnetic fields present. Collisions between neutrals and charged particles, though statistically of low probability, are modeled.

—The plasma is pseudo-electrostatic—the earth's magnetic field is roughly constant over the time of the simulation which covers no more than 2 sec. of time of a satellite in orbit. Consequently, the time rate of change of the earth's magnetic field was not included in this stage of development of the simulation. Thus, it is assumed that

$$\frac{\partial \mathbf{B}}{\partial t}=0. \quad (5)$$

The equations governing the motion of the particles reduce to the Newtonian form,

$$m\frac{d\mathbf{c}}{dt}=\mathbf{F}. \quad (6)$$

where

$$\mathbf{c}=\frac{d\mathbf{x}}{dt}, \quad (7)$$

and the Lorentz force has two components,

$$\mathbf{F}=\mathbf{F}_{\text{ELECTRIC}}+\mathbf{F}_{\text{MAGNETIC}}=q\mathbf{E}+q(\mathbf{c}\,X\,\mathbf{B}), \quad (8)$$

with q as the particle charge, $\mathbf{E}$ as the electric field, and $\mathbf{B}$ as the magnetic field. Due to the electrostatic plasma assumption, $\mathbf{B}$ can be assumed constant. A solution for the $\mathbf{E}$ field is thus required to move the particles. Once again, the electrostatic plasma assumption is involved and implies

$$\nabla X\,\mathbf{E}=-\frac{\partial \mathbf{B}}{\partial t}=0, \quad (9)$$

such that

$$\mathbf{E} = -\nabla\varnothing, \tag{10}$$

where $\mathbf{E}$ is the electric field potential. We also have

$$\nabla \cdot \mathbf{E} = \frac{\rho}{\varepsilon_0}, \tag{11}$$

where ρ is the charge density and ε_0 is the permissivity of free space. Combining (10) and (11) yields

$$\nabla^2\varnothing = -\frac{\rho}{\varepsilon_0}. \tag{12}$$

The consequence is that, given the assumptions of the flow in LEO, the Poisson equation presented in Eq. (12) will adequately model the $\mathbf{E}$ field conditions. Computationally, the charge density is accounted for by allocating a proportionate amount of the charge of a given charged particle to the eight nodes on the corners of its cell. The $\mathbf{E}$ field is then obtained using Eqs. (10) and (12). The particles are then moved within the grid structure until the $\mathbf{E}$ field is stabilized.

Collisions between neutrals and charged particles are modeled using similar methods to those employed for neutral–neutral collisions. An ion collision cross section is established and the appropriate collisions are statistically selected. Charge transfer is allowed and treated as a chemical reaction.

2.3. *Spacecraft Charging Simulation*

The equation for spacecraft charging, in terms of the current densities, is

$$J_E(V) - (J_I(V) + J_{BSE}(V) + J_{PH}(V) + J_B(V) + J_{SI}(V) + J_{RLC}(V)) = J_T(V), \tag{13}$$

where

V = spacecraft potential,
J_E = ambient electron flux to a point on the spacecraft surface,
J_I = ambient ion flux to a point on the spacecraft surface,
J_{SE} = secondary electron flux due to J_E,
J_{SI} = secondary ion flux due to J_I,
J_{BSE} = backscattered electrons due to J_E,
J_{PH} = photoelectron flux,
J_B = active current sources, and
J_{RLC} = resistive, capacitive and inductive coupling currents between a point and an adjoining surface.

The fluxes J_E and J_I are modelled using discrete-particle simulations and trajectories. Full electronic accommodation is assumed. Investigation of J_{SE} indicates that the effect peaks at releasing 0.8 secondary electrons per 300 eV electrons (see Smith and West, 1983; Jursa, 1985). As Rawer states (1981), the LEO electrons are typically much less energetic than this, and since the effect is negligible J_{SE} is not modelled. Investigation of J_{SI} indicates that the effect peaks at 5 per 20,000 eV ion. Rawer (1981) also found that the LEO ions are much less energetic than this; thus, J_{SI} is not modelled. Smith and West (1983) found that the magnitude of J_{BSE} indicates that the effect of backscattered electrons is negligible for an incident electron below 100 eV. As the LEO electrons are typically much less energetic than 100 eV (see Rawer, 1981) and since the effect is negligible, J_{BSE} is also not modelled. The photoelectron flux can be modelled as a boundary condition, but for the purposes of this investigation the sun was assumed to be shining directly on the edge of the flat disk; consequently, this effect was not modelled. Current sources can be modelled as streaming, discrete electrons, but for the purposes of this investigation this effect was not modeled. Finally, the spacecraft modeled is a solid stainless steel disk. Consequently, J_{RLC} is zero. Thus, for the purposes of this investigation, the assumption is made that the spacecraft charge is only a function of the difference between the ion and electron fluxes. It is understood that a more rigorous charging model is required for a more complicated spacecraft.

3. ACCURACY OF THE CODES

The accuracy of a Monte Carlo code is very dependent on the physics which are included in the molecular representation and does not directly compare to the accuracy in solving a specific governing differential equation. The fact that a specific macroscopic phenomenon can be deduced from a direct solution technique of a governing equation does not hold true for Monte Carlo codes. For a specific macroscopic result to be observed (i.e., pressure), an accurate representation of its microscopic behavior must occur (i.e., number densities and energy states). Consequently, a Monte Carlo simulation will accurately simulate only those macroscopic phenomena which have, as their basis, accurately modelled microscopic phenomena. The DSMC codes will fluctuate about a statistical mean for a given phenomenon. The standard deviation of the expected fluctuations is approximately equal to the square root of the sample size. Another view is that the program will converge as the inverse of the square root of the sample size. Thus, the accuracy of a DSMC code is not tied to the classical references for spatial and temporal accuracy, but is more properly tied to the question of sample size and number of samplings, which are discrete values chosen by the investigator. In most plasma simulations, the investigator is less interested in the accuracy of the individual particle orbits and is more interested in the accuracy of the collective plasma phenomena. In this investigation, the particle trajectories are the precise phenomena which are of interest, which leads to the particle density distribution throughout the flow field, particularly in the near wake. The CARLOS code uses a fast Poisson solver to generate the electric field, using the techniques previously discussed. These techniques yield a second-order correct spatial accuracy. The temporal accuracy

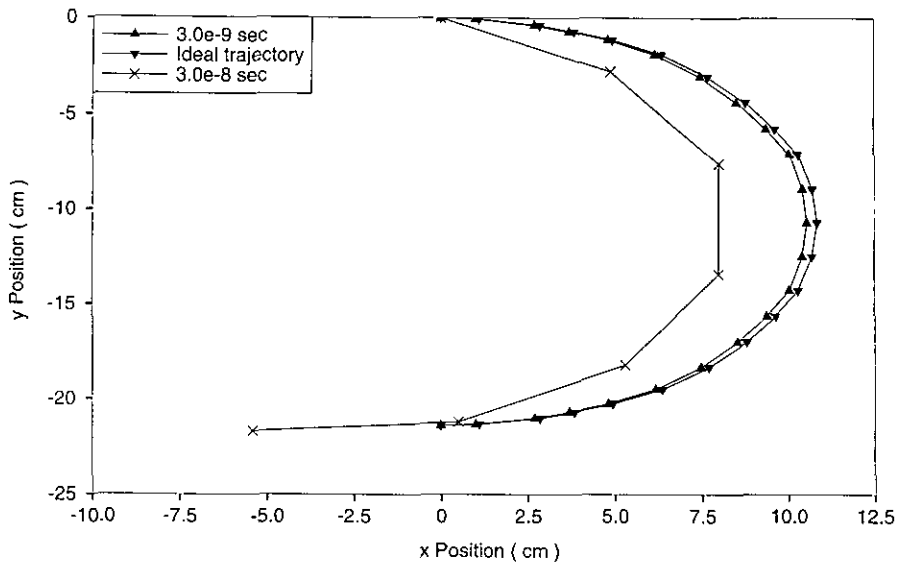

FIG. 1. Cyclotron radius of a 10 eV electron moving in the presence of an orthogonal 1 gauss magnetic field through what should be a half cyclotron period (×, 3.0 e^{-8} sec.; ▲, 3.0 e^{-9} sec.; ▼, ideal trajectory).

of the technique is limited by the particle-move process in the presence of a magnetic field. The particle-move process uses a leapfrog technique which yields a particle-trajectory phase error which is proportional to $N(\omega_0\Delta t)^3/24$, where N is the step number and ω_0 is the cyclotron frequency. If one were to consider the presence of a magnetic field, the particle-mover position error becomes first order in time and is proportional to $\omega_0\Delta t/2$. Consequently, the time step would be limited by the particle-mover position error.

This situation is illustrated in Fig. 1 with a plot of the results of two different time steps of a 10eV electron moving in the presence of an orthogonal 1 gauss magnetic field through what should be a half cyclotron period. It is noted that both the optimum and the nonoptimum trajectories display good phase matching. At the end of one-half of a period, both indicate a trajectory which is approximately parallel to the horizontal axis. However, the position error is evident in that the difference in the nonoptimum position and the ideal position is 0.5 cm. The position error in the optimum case, although slight, is still noticeable.

The effects of different molecular models were considered. The use of a VHS molecular model was examined based on degree of simplification and also because physical effects could be obscured with this model.

Previous computational investigations have been conducted to examine the problem of collisional molecular flow, and a great deal of experience has been accumulated on the effects of the molecular model on low density flows. It was found that the observed molecular effects could be correlated with the change of the differential cross section of the particles with respect to the relative velocity. This suggested that the form of deflection angle scattering and attractive forces of neutral particles was not important and led to the VHS model. Consequently, the VHS model was used in this investigation.

3.1. *Convergence*

The term convergence as used in this section indicates that the solution of the computational equation in the limit converges to the governing partial differential equation as the time step and the grid size become infinitely small. For a DSMC code, it has been proven that, in the limit, the algorithm converges to the Boltzmann equation for a weight factor of one. Convergence with other weight factors becomes a statistical question and is no longer concerned with the governing equation. Specifically, the process in question is a statistical Poisson process which will converge as the inverse of the square root of the sample space and must be investigated for convergence boundaries (i.e., minimum number of time steps for a given number of simulated particles).

The rate of convergence of the CARLOS code was investigated and compared to the runs generated by Bartel (1991) at Sandia National Laboratories (SNL). The SNL code uses a DSMC method due to Bird (1976, 1978, 1981) and modified by Bartel. The CARLOS code is a three-dimensional code which has two separate computational grids overlaying each other while the SNL/DSMC code has only one two-dimensional grid. Thus, our 20 × 20 × 20 neutral-particle grid has approximately the same computational overhead as a 16,000-cell two-dimensional SNL code. As the cell count is typically much lower than 16,000, it is not considered computationally expensive to run the two-dimensional code through a very large number of time steps. Thus, the present code normally will not generate the number of time steps used in the SNL/DSMC code. This is strictly due to computer time constraints. Our

TABLE I

Typical CPU times (sec. on a CRAY XMP[a])

	250 km	500 km
Neutrals only	34,601	26,944
Charged only	57,693	56,989
Full flow	142,623	101,404

[a] 20 × 20 × 20 neutral grid, 32 × 32 × 32 EM grid, 40 particles per neutral cell maximum, 600 time steps.

CPU times are shown in Table I. Typically, the present code will run from 100 to 1,000 time steps while the SNL/DSMC code will run from 1,000 to 50,000 time steps. Note that the size of our charged-particle grid was 32 × 32 × 32.

A series of runs was made, varying the number of time steps in the code. The number density along the disk axis of symmetry is plotted for 10 and 100 time steps (Fig. 2). These are plotted against a 40,000-time-step run of the SNL/DSMC code. The results from the runs converge very rapidly to the SNL/DSMC case. This agrees well with the theoretical convergence of a DSMC code (i.e., proportional to the inverse of the square root of the number of samples). All parameters investigated for the 10-time-step through the 100-time-step cases exhibited the same rapid convergence.

4. COMPARISONS

The discrete particle code was investigated at the low end of the LEO environment (250 km) and at the high end of the LEO environment (500 km). Before discussing the results obtained, some remarks concerning the accuracy of existing experimental data, to which comparisons are desired, are relevant. Existing measurements of the wake structure around spacecraft in LEO were not intended to obtain high resolution data in the near wake regions which is the goal of this work. The orbital measurements taken by the various satellites have had an error band of ±10 to ±40% of the total number density along with an atmospheric variability of ±20 to ±80%. The species breakdown and energy states show error bands measured in orders of magnitude. An investigation was made to determine if any orbital data (Marcos, 1990) could be compared favorably with computational results. Figure 3 displays the result of this investigation. Total number density was used as the basis of this investigation as this was considered to be the measure with the smallest error band. The upper and lower curves depict the ±20% total number density variation from a full flow case. Specifically, flow in the presence of a magnetic field and a reduced thermal accommodation case were added to the full flow and neutral cases. It is significant, though, that these test cases all vary radically in their results; they all lie within the error bands of today's capability of measuring the free stream number density. Due to the results of this investigation, comparison to orbital measurements were not done. The first space experiment to explore the ultra-vacuum environment will be the WSF, and these experimental data are yet to come. To date, no terrestrial wind tunnel is capable of duplicating the LEO environment.

4.1. *Comparison of the Discrete Particle Code to SNL/DSMC*

The discrete particle code was verified by comparison to the SNL/DSMC code. Two test conditions were chosen. The first

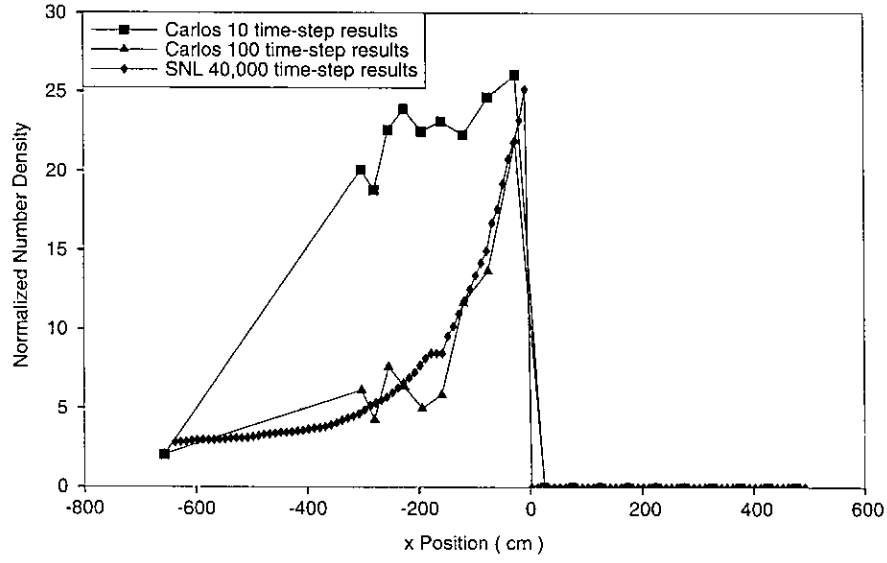

FIG. 2. Number density normalized to the free stream condition. Comparison of SNL 40,000 time step results (♦) to the CARLOS 10 time step results (■) and 100 time step results (▲).

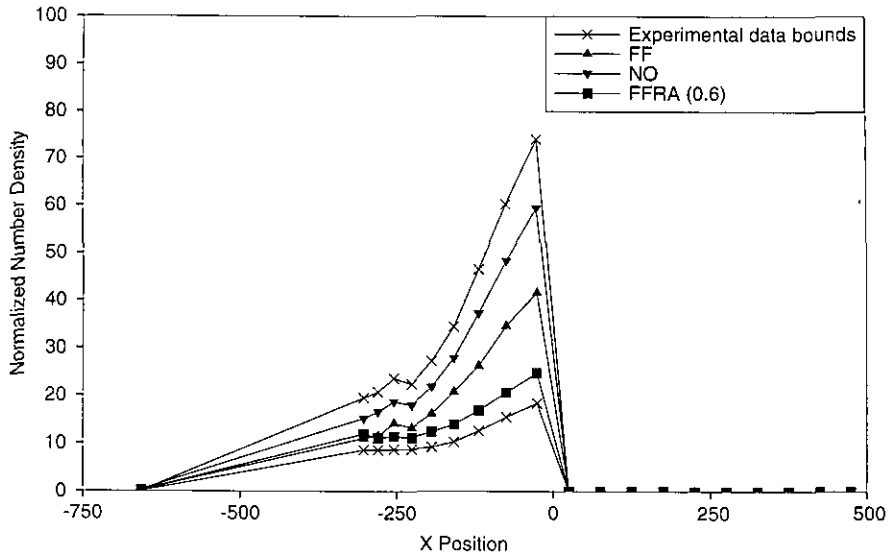

FIG. 3. Comparison of various flow conditions and the error expected of orbital measurements at 250 km. (▼, neutrals only; ▲, full flow; ■, 0.6 thermal accom.; ×, upper and lower bounds of experimental data).

test scenario was chosen at 250 km as this is approaching the lower limit of LEO space. This orbital altitude yields a case where the equilibrium value of the undisturbed state is fairly collisional and densification regions will be collisionally dominated. These conditions allow the comparison of the two codes in areas where the flow is collisionally dominated. The second test scenario was chosen at 500 km as this is approaching the upper limits of LEO space for the vehicle of interest (i.e., STS). This orbital altitude yields a case where the equilibrium value of the undisturbed state is essentially a free molecular flow for the purposes of the computation. However, more collisional regions along the ram side will allow comparison of densification rates.

The present code (CARLOS) was run as a three-dimensional code while the SNL code is a two-dimensional code. Consideration was given to running the present code as a two-dimensional code to reduce the number of differences between the two codes. This was not done for several reasons, the most important of which is that CARLOS is run in three dimensions when doing a full flow simulation, thus the mode to test is the three-dimensional mode. Also, the special gridding to make the simulation two-dimensional would be difficult to match for the charged particles, raising the question as to whether a two-dimensional mode is equivalent to a three-dimensional mode based on the analysis herein.

Two runs were made to compare those with results with the SNL code. The two codes have differing methods of data entry and condition setting; however, every attempt was made to match the input parameters, boundary conditions, and statistics-gathering algorithms. In this manner, any differences noted would indicate an algorithm disparity pointing to a discrepancy in modeling the physics of the problem. As will be presented later, the two codes matched well within the statistical scatter of a Monte Carlo based code which is inversely proportional to the square root of the sample size.

The SNL code is most valid on the ram side; therefore, number density, internal temperature, and translational temperature are compared. Detailed comparisons are made using the values along the axis of symmetry of the wake shield model.

In this investigation, our 250 km runs allowed cloning, whereas our 500 km runs did not allow cloning. In both cases, the SNL code allowed cloning. Figure 4 compares the generated number densities at 250 km. These plots are normalized to the undisturbed equilibrium number density. The SNL code generated a densification of approximately 25 times the undisturbed condition. Our code generated a densification of 23.6 times the undisturbed condition, displaying good agreement with the SNL code. Also, the densification anomaly, often referred to as the bow wake phenomenon, is noted to have occurred at 240 cm upstream in our results while the SNL results placed the anomaly at 210 cm. The wake side in both cases displayed no rise in the number density for 500 cm even when the raw data were examined. This is a nonphysical result of the cloning/decloning process. A similar agreement was found in the 500 km calculations.

Our generated internal temperature and the SNL generated internal temperature at 250 km are compared in Fig. 5. The slope of each set of results on the ram side shows reasonable agreement. The maximum values also compare well. In the wake region, the SNL code indicates no internal temperature until almost 400 cm downstream. Our code displays a low internal temperature until approximately the same distance. After this point, both codes indicate an increase to approximately the same value. Both results in the wake region must

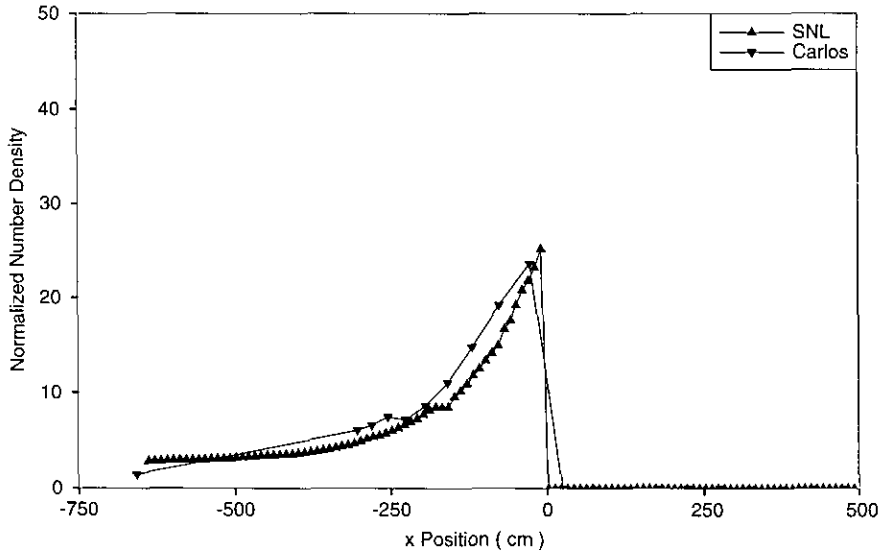

FIG. 4. SNL generated number density vs CARLOS generated number density along the axis of symmetry at 250 km. Both sets of results have been normalized to the undisturbed equilibrium condition (▼, CARLOS; ▲, SNL).

be considered suspect due to cloning. Specifically, the trajectories of the particles are altered from what would have been their true trajectory. They are decloned in an artificial manner which attempts to model the physics of a highly coupled flow regime simply and quickly. Information has been lost in the cloning process which is not retrieved when a particle in question is decloned into smaller particles. The region in the near wake is dominated by these decloned particles and consequently reflects the artificially imposed physics.

The two generated internal temperatures at 500 km are compared in Fig. 6. The maximum values at the wake shield ram face agree well. On the wake side, the SNL code generated an anomalous point at approximately 125 cm. Our CARLOS code, which did not use cloning in its calculations, indicated a consistently low internal temperature across this range. This fact, along with a low number density as shown in Fig. 6, indicates that the diatomic particles are relatively few, but of very high energy.

The two generated translational temperatures at 250 km are compared in Fig. 7. The slope of each set of results on the ram

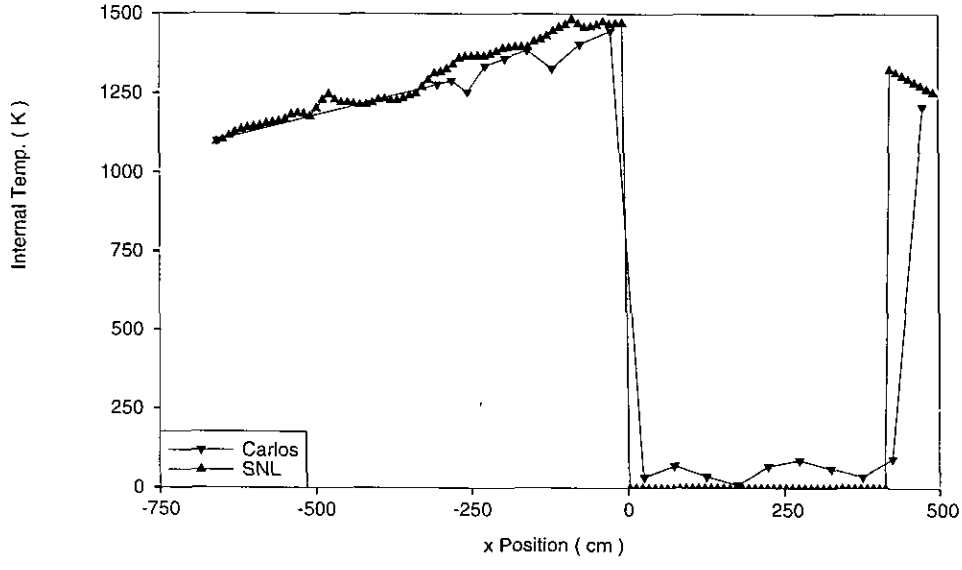

FIG. 5. SNL generated internal temperature (K) vs CARLOS generated internal temperature (K) along the axis of symmetry at 250 km (▲, SNL; ▼, CARLOS).

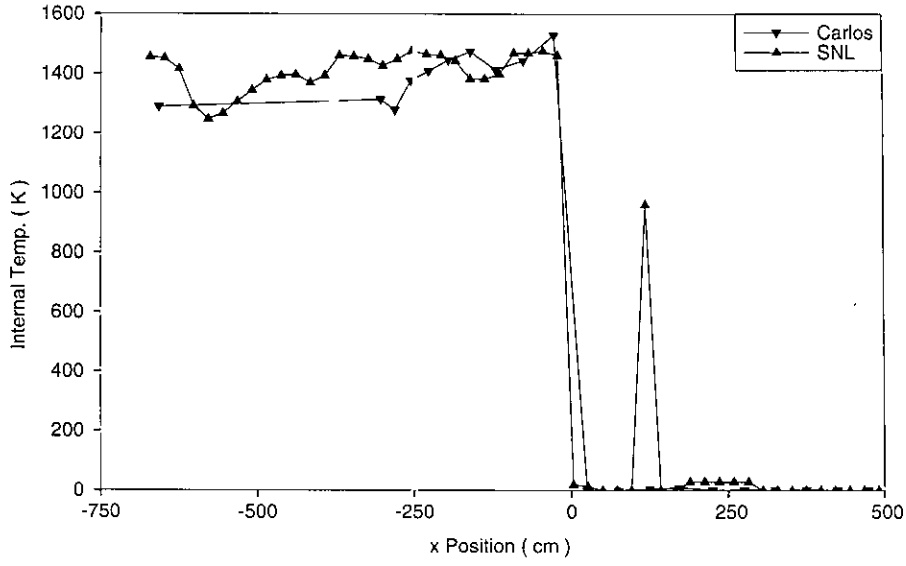

FIG. 6. SNL generated internal temperature (K) vs CARLOS generated internal temperature (K) along the axis of symmetry at 500 km (▲, SNL; ▼, CARLOS).

side shows good agreement. The maximum values also compare well. On the wake side, the SNL code displayed a spike at approximately 125 cm. This spike aligns with the spike previously discussed in the 500 km internal temperature case. For an anomalous spike to exist at this same location in two radically different flow conditions tends to point to a nonphysical simulation during the decloning process. Our results, which used a different decloning process, displayed a gradual rise in the translational temperature across this region. While this result may appear more physical, the data are still suspect due to decloning. Both runs would indicate a very low translational energy state in the area of the near wake whereas the theory of drifting Maxwellian gases would imply that this area would be mostly populated by very high energy particles of the lighter species entering the computational field from the downstream side of the disk and the reflected particles of this type (thermally accommodated) which have experienced a collision with the wake surface of the disk (see Chapman and Cowling, 1970). As the particles with a higher speed would spend less time in a given computational cell than their thermally accommodated counterpart, a steady increase in energy with distance from the disk on the wake side is anticipated.

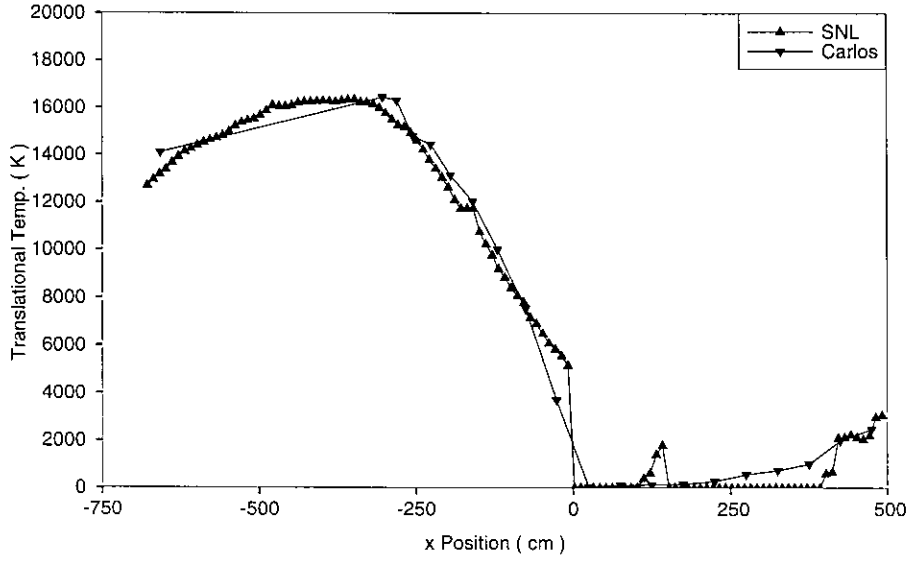

FIG. 7. SNL generated translational temperature (K) vs CARLOS generated translational temperature (K) along the axis of symmetry at 250 km (▲, SNL; ▼, CARLOS).

The case depicted in Fig. 7 was treated at 500 km. The maximum values at the disk ram face showed good comparison. On the wake side, the SNL code generated the same spike at approximately 125 cm. Our CARLOS code generated results which displayed a steady increase in energy with distance from the disk. This fact, along with the number density results at 500 km, indicates that the steady increase is the same behavior as described in the previous paragraph.

It can be seen by the comparison of the results from these two codes at these two altitudes that the internal and external energy states display excellent agreement and the number density is matched well along the axis of symmetry on the ram side.

4.2. *Comparison of Charged Particle Code to POLAR*

Our description is unique from other plasma models for several reasons. One of these reasons is that it is particle-based and focuses more on the particle phenomena than the overall plasma phenomena. Specifically, this investigation centered on the number density in the near field of a charged spacecraft and the energy states in the near field. With this in mind, the particle number densities and the field that affected the particle trajectories were considered as the most important of all the possible results to compare. Thus, our **E** field, as described earlier, which is the final product of the field-solver technique, is compared to the **E** field generated by the POLAR code (Katz *et al.*, 1989) which was generated by the U.S. Air Force Phillips Laboratory and verified through comparison with plasma tunnel data. Also, the number density of each particle species is compared to the number density generated by the POLAR code.

The charged particle portion of our approach was verified against the POLAR code. Two test conditions were chosen. The first test scenario was a 250 km case with appropriate plasma number density and orbital velocities. The second test case was similarly chosen at 500 km. The runs were made with a 0.5 mole fraction for N^+ and O^+.

A major change to the wake shield model as implemented in our code was required for commonality with POLAR. The wake shield had to be modeled as an octagon with thickness since the POLAR code is restricted on the geometries it can simulate. In general, POLAR cannot model a shape that is not a buildup of cubes and wedges. Also, the grid points where the results were compared are identical between our code and POLAR.

Finally, the charge on the shield was forced to be equal in both codes to avoid any errors generated due to different charging algorithms. This turned out to be unnecessary as the charge values were very comparable. Of the ten runs compared, the worst case was -1.52 volts for our code vs. -1.542 volts for POLAR at 250 km and -1.201 volts for our code and -1.19 volts for POLAR at 500 km.

The electric fields generated by the two codes were compared. The maximum difference in magnitude occurred closest to the wake shield ram face. A search of the results files on a point-by-point basis revealed a maximum difference of 2.6% at 250 km and a 2.4% difference at 500 km. Figure 8 shows the normalized percent difference at 500 km. The normalized percent difference values at 250 km were virtually identical. Both comparisons show that the greatest difference occurred at the edges while the difference along the ram and wake face stayed close to 0.6%.

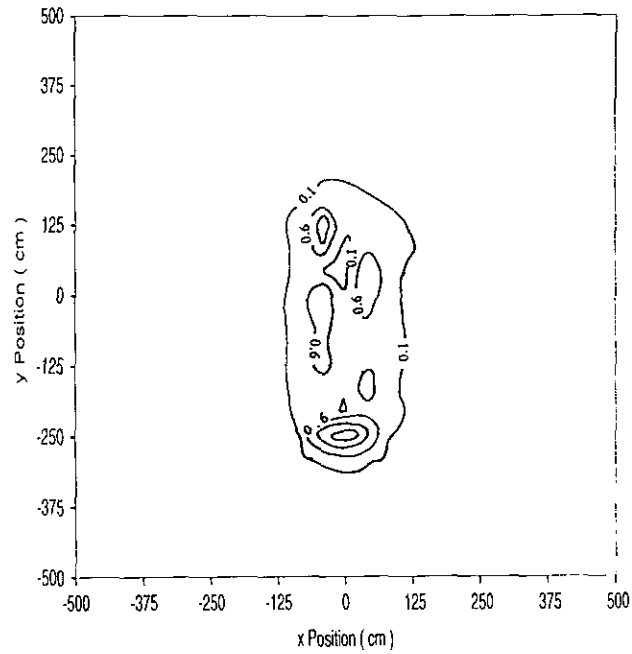

FIG. 8. *Normalized percent error of E field magnitude at 500 km along central plane (POLAR vs CARLOS).*

A major difference in the manner that our code handles the particles versus the POLAR method is that our code considers the boundaries as reentrant. This implies that the particles can enter from any of the six computational boundaries as opposed to POLAR which uses a reverse trajectory method. Also, the graphics package used attempted to enforce closure by forcing the solid line plots to curve in toward each other between the graphics boundaries and the data point closest to the graphics boundary. Consequently, the pinching effect noted on all graphs close to the right or left side of the plots is a graphical artifact and is thus not a physical phenomenon. Figures 9a and 9b compare the isodensity contours for the two codes at 250 km. The 0.2 ion density, Fig. 9a, matches well, indicating a 20 cm mismatch between the two codes at 170 cm. The 0.4 ion density case (not shown) has a better match at 170 cm, indicating a difference of 10 cm. The 0.6 (not shown) and 0.8 (Fig. 9b) ion densities display excellent matching in the 50 cm to 450 cm region. Figure 9b displays the graphics anomaly previously discussed. The plotting package used to plot our results attempts to find closure, giving the impression of the isodensity trace pinching together prematurely. Both the POLAR and CARLOS plots display a dominance of the ram flow (i.e., an orbital

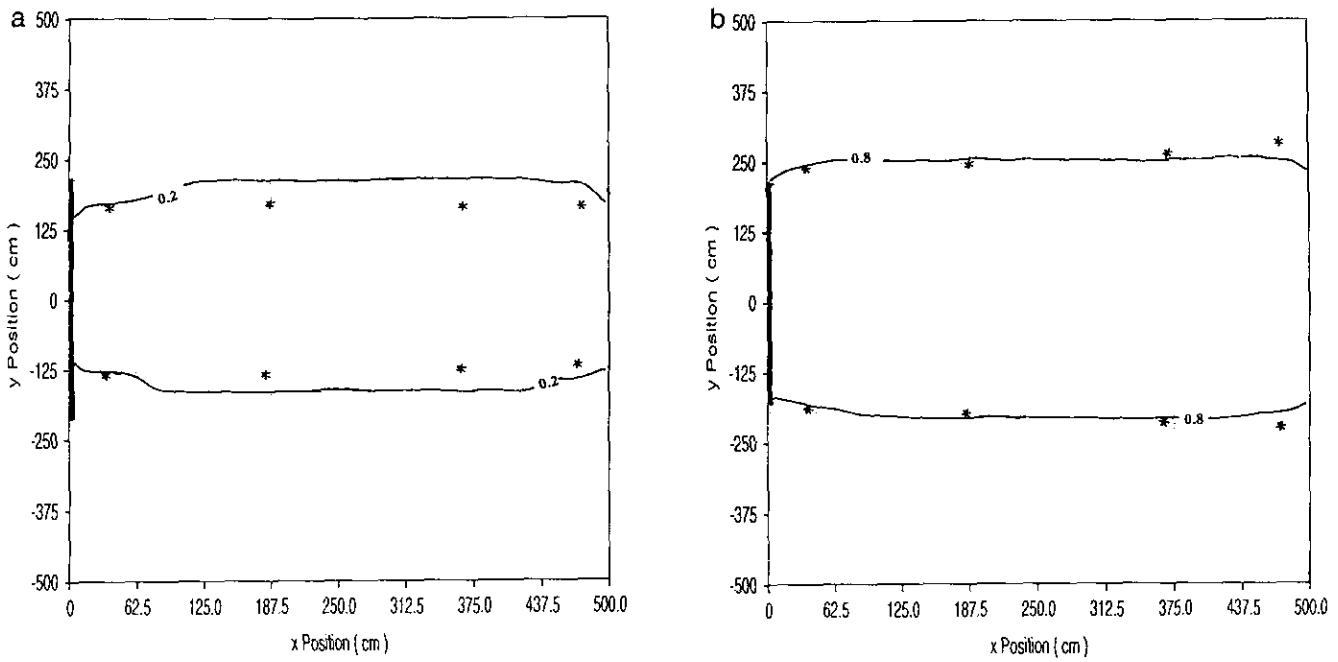

FIG. 9. Ion density comparison at 250 km. (a) 0.2 ion density, (b) 0.8 ion density; (—) CARLOS, (*) POLAR.

velocity component of 7.7 km/sec superimposed on the particle's thermal velocity component) as indicated by ion density tracks aligning roughly with the disk edges. Also, it should be noted that the gradient is very steep from 0.2 ion density to the 0.8 ion density, once again indicating the dominance of the ram flow over the electromagnetic effects.

The 500 km runs were done using 500 time steps past the point where statistical variations were minimized as opposed to the 1000 time steps used in the 250 km case. Figures 10a and 10b compare the isodensity contours for the two codes at 500 km. All four of these ion density comparisons display good matching. The 0.4 ion density case in Fig. 10a displays a good match at 170 cm, indicating a difference of 8 cm. The 0.6 ion density values in Fig. 10b display excellent matching in the 50 cm to 450 cm region. Similar agreement was obtained for the 0.2 and 0.8 ion density calculations; however, these results are not shown here. Figures 9 and 10 display a dominance of the ram flow as indicated by ion density tracks aligning roughly with the disk edges.

The atmospheric conditions present in the LEO environment are highly variant, as described earlier. Recognizing this situation, a sensitivity investigation was considered appropriate. The major factors which can be expected to change on a given orbit with respect to the charged particles are the ion number density, the ion temperature, and the electron temperature. This effect is mostly due to diurnal variation, but can also be expected to occur due to atmospheric variations as well. The variation of altitude in LEO space appeared to have little effect on the **E** field; consequently, the ion density plots display a great deal of similarity.

The sensitivity investigation of varying ion number density for a given temperature was considered to be accomplished in the two runs previously discussed in this section where the ion temperature was approximately constant, but the number density changed by an order of magnitude with the results as previously discussed. Consequently, the sensitivity of the solution with respect to the ion and electron temperatures was evaluated. Three runs were made to evaluate the effect of the **E** field with respect to varying temperatures. The runs were accomplished at 250 km with the temperatures simulating a warm plasma that had an ion temperature of 1300 K and an electron temperature of 2100 K, a normal plasma that had an ion temperature of 1000 K and an electron temperature of 1800 K, and a cool plasma that had an ion temperature of 710 K and an electron temperature of 1100 K. These values for the ion and electron temperatures were considered representative and were taken from the *International Reference Ionosphere* (see Rawer, 1981).

Calculations have been done for the **E** field for the three different plasma cases mentioned in the previous paragraph. The normal plasma results are shown in Fig. 11 while the warm and cool plasma results are not shown. The contour lines indicate the **E** field magnitude in volts/m. The primary effect expected was that of the **E** field scaling with the equilibrium temperature. The **E** field should be stronger and be more extensive for the warmer plasma. Comparison of the 0.5 volt/m contour between the three cases displays this effect. In the warm plasma case, the field is the strongest and the 0.5 volt/m contour extends into the wake region to approximately 450 cm. The normal plasma case depicted in Fig. 11 shows the 0.5

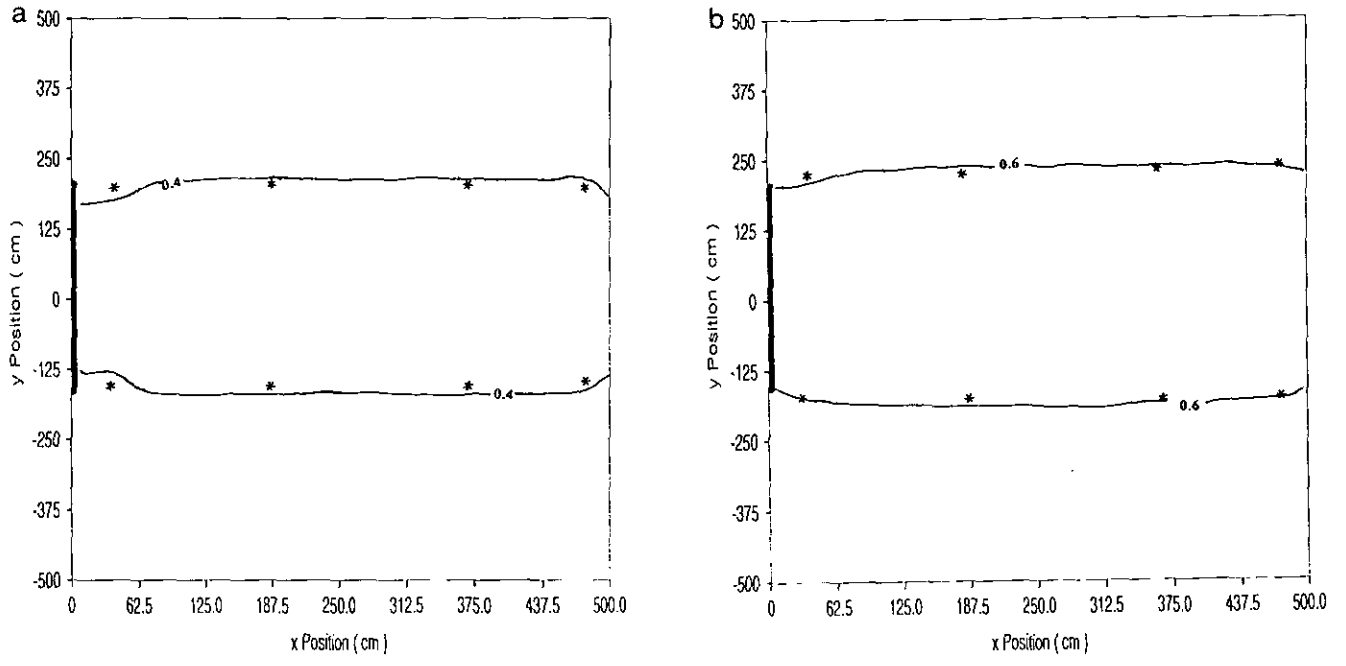

FIG. 10. Total ram side number density at 500 km. PlasmaOn option is enabled: (a) 0.4 ion density, (b) 0.6 ion density; (—) CARLOS, (*) POLAR.

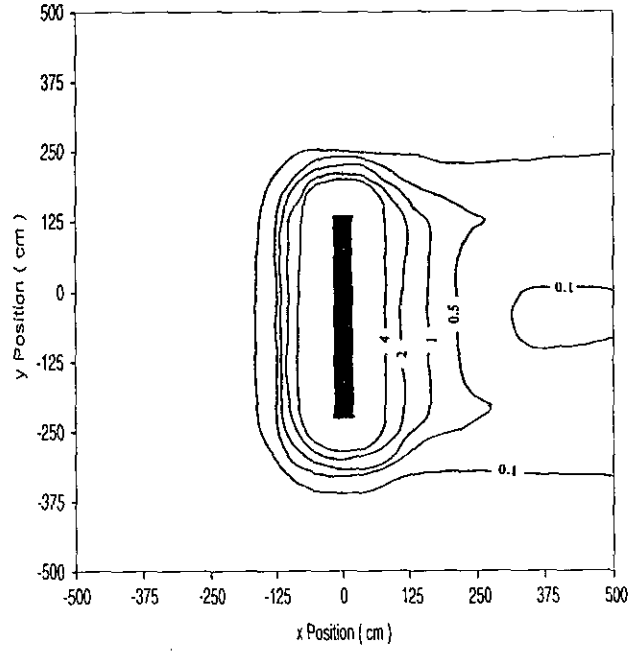

FIG. 11. Topographical plot of the E field magnitude (v/m) of a normal LEO plasma at 250 km. Ion temperature is 1000 K and electron temperature is 1800 K.

volt/m contour extending approximately 270 cm into the wake region while the cool plasma case has the 0.5 contour line extending approximately 170 cm into the wake region. The position of the innermost contour line plotted also is revealing, although the effects are more subtle. The warm plasma topographical plot displays the 4 volts/m contour line displaced approximately 100 cm from the ram face. The normal plasma result has the 4 volts/m contour line approximately 6 cm closer to the ram face than the warm plasma case. The cool plasma topographical plot displays the 4 volts/m contour line approximately 16 cm closer to the ram face than the warm plasma case. These three cases display the anticipated response in their respective environments.

The wake is anticipated to be slightly modified by the different **E** fields. The warm plasma should display a slight pinching of the positive ion wake as compared to the cool plasma. In all cases, the ram flux should prove to be a dominant factor.

5. FULL FLOW CODE

The present code was designed to resolve the flow structure of an orbiting spacecraft. Specifically, it has been designed to resolve the near field phenomenon in LEO. To accommodate this study, there are several differences in the our code which make it unique when compared to other codes. First, the charging of the vehicle is done in concert with the particle-in-cell (PIC) simulation on both the ram and the wake face of the computational model. Also, the **E** field is stabilized in concert with the neutral-particle-collision process. In this manner, the

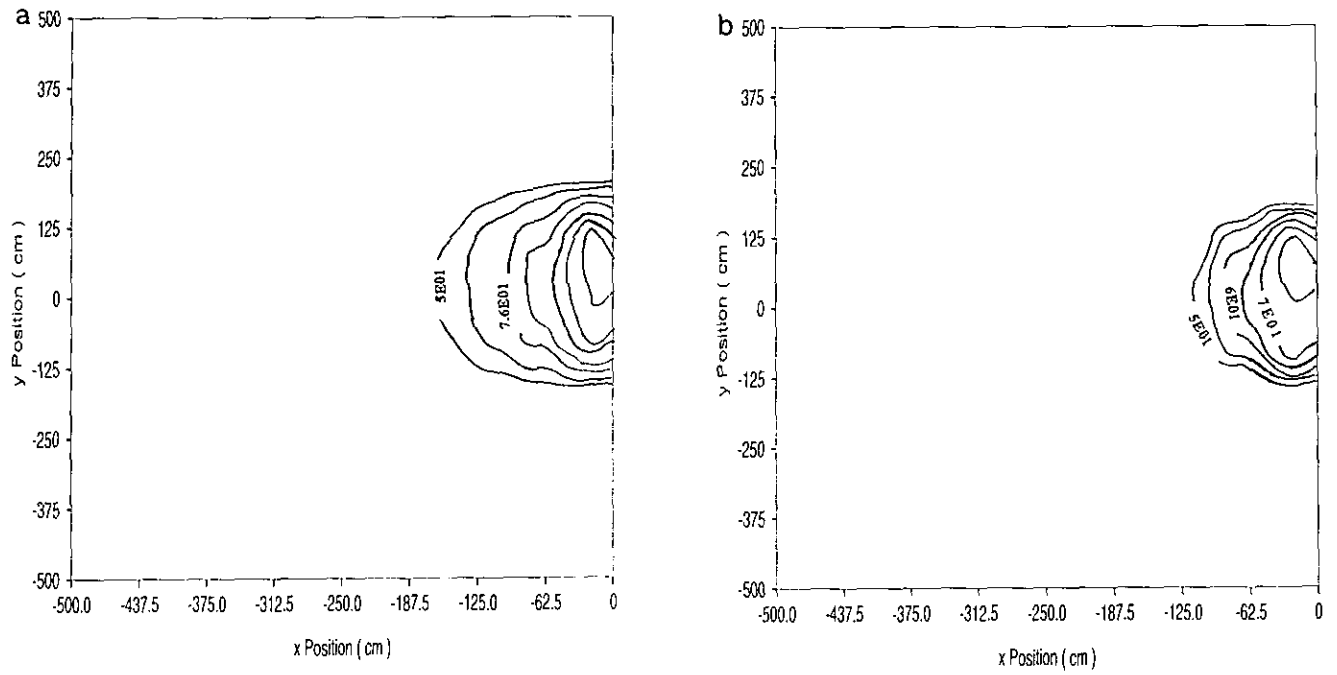

FIG. 12. Total ram side number density at 250 km (5.0E9 contours and 1000 cycles): (a) PlasmaOn option is disabled, (b) PlasmaOn option is enabled.

Boltzmann phase space of the plasma is modified by both the neutral collisions and the aerothermochemistry. Further, the atomic particles are introduced in a proportional population manner on all six computational boundaries. In this way, even the effects of the minor species can be noted on the computational domain.

Recent studies indicate that the thermal accommodation at the surface is not as has been previously modeled. Specifically, the energy states, upon surface impact, are more fully accommodated than previously suspected, but there is a notable number of specular events. The physics-modeling within the code can account for this phenomenon.

One of the simplifications which allows a DSMC code to model a chemically reacting, weakly ionized plasma is its ability to track the produced electrons along the same trajectory as its associated parent ion. In this context, an aerothermochemistry-produced electron or simply a produced electron is any electron which enters the computational domain due to an ionization event within the computational boundaries. This technique has been used to predict flows through auroral regions and reentry flows. The justification for this simplification is that the flow characteristics of interest to the investigation do not include ions or electrons. Our code does not track the charged particles in this manner. Instead, our code generates and stabilizes an electromagnetic field and then moves the charged particles through the field according to the appropriate equations of motion.

The effect of produced electrons at 250 km is shown in Figs. 12a and 12b. The number density in this case includes the produced electrons. It is noted that if produced electrons and ions are included, there will be a significant overestimation of number density. Consequently, if the investigation is attempting to yield results which include charged particles in the presence of an **E** field (i.e., electron number density behind a reentry shock wave or ion/electron return flux), the number density will be significantly in error. Since the results which are of interest to a near-field study include the separation of the ion/electron pair in the presence of electromagnetic fields, this simplification was not considered appropriate.

Reproducible experimental results of thermal accommodation at orbital energies has been unavailable until recently. Of paramount importance is the thermal accommodation of atomic oxygen from typical spacecraft surfaces. Very recently (through Krech *et al.*, 1991), the technology has become available to generate a 5 eV atomic oxygen stream to study its accommodation on engineering surfaces. Prior to this study, Bird (1976, 1978, 1981) had assumed full accommodation even though it was generally understood (through Knox *et al.*, 1991) that the accommodation was less than full. In the absence of solid data, most investigators (Bird, 1976) chose to err on the conservative side.

Figure 12b also depicts the ram side total number density with full thermal accommodation while Fig. 13 depicts the ram side total number density with a reduced thermal accommodation. Whereas it is noted that the symmetry of the densification is not affected, the amount of densification is greatly affected. Figure 14 displays this densification along the axis of symmetry. It is significant that the normalized number density varies from

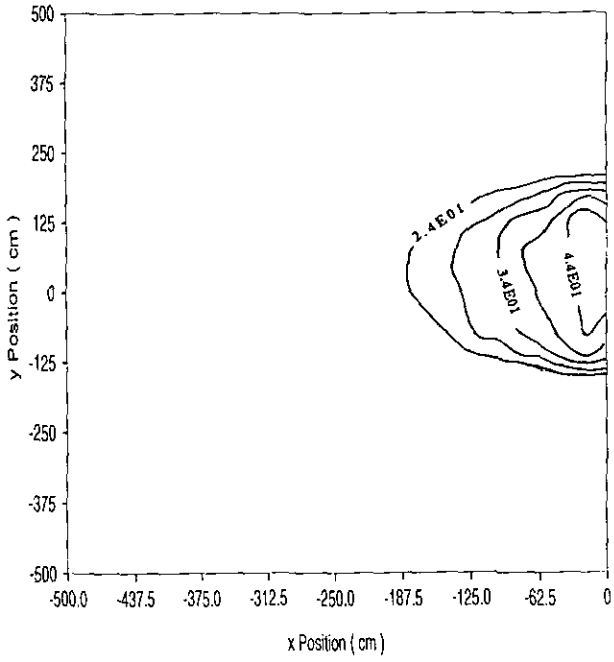

FIG. 13. Ram side total number density with a reduced thermal accommodation for full flow at 250 km (0.6 accommodation, 1000 cycles, 5.0E9 contours).

59 in the neutral-only case to less than half of that value, 23, in the reduced-accommodation case. Figure 15 displays the effective translational temperature along the axis of symmetry.

It is significant that this plot indicates that the molecular state stays at a higher energy level with reduced accommodation. This is due to the fact that approximately 40% of the particles which experience a gas–surface interaction are reflected specularly with no change of energy state. Thus, the effective translational temperature (i.e., with respect to the disk) rises from approximately 23,000 K for the full accommodation case to 33,500 K for the reduced-accommodation case.

An important point to note from this investigation is that, even though the ram side conditions varied widely as discussed above, the wake isovalue plots did not reveal that marked a difference. While the ram side case displayed a significant (over half) reduction in number density, the wake side case depicts no discernible differences. Comparison of the wake side plots of all other cases run displayed the same lack of discernible differences. These results are not shown here.

6. CONCLUSIONS

A full flow simulation computer code has been generated and validated for a range of low earth orbit undisturbed equilibrium conditions by direct comparison to available computer codes within the valid range of each of these respective codes. It has been demonstrated that macroscopic and microscopic properties of nonequilibrium orbital flows can be predicted from the interparticle potentials and undisturbed equilibrium conditions. Also, the flow field properties were investigated for sensitivity to electromagnetic fields, aerothermochemistry, and collisional dependence.

Several conclusions can be drawn from this effort:

1. A technique was developed and a tool was produced to solve the class of problems containing a charged structure in a LEO plasma and was benchmarked where possible.

2. The use of advanced data structures on a supercomputer

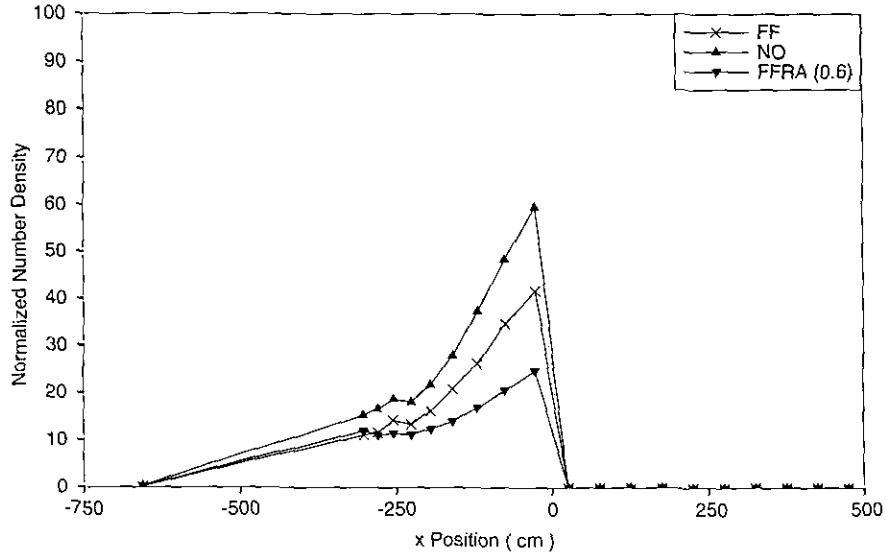

FIG. 14. Comparison of normalized total number density along the axis of symmetry at 250 km: (▲) neutrals only flow, (×) full flow case with full accommodation, (▼) full flow with a reduced (0.6) accommodation.

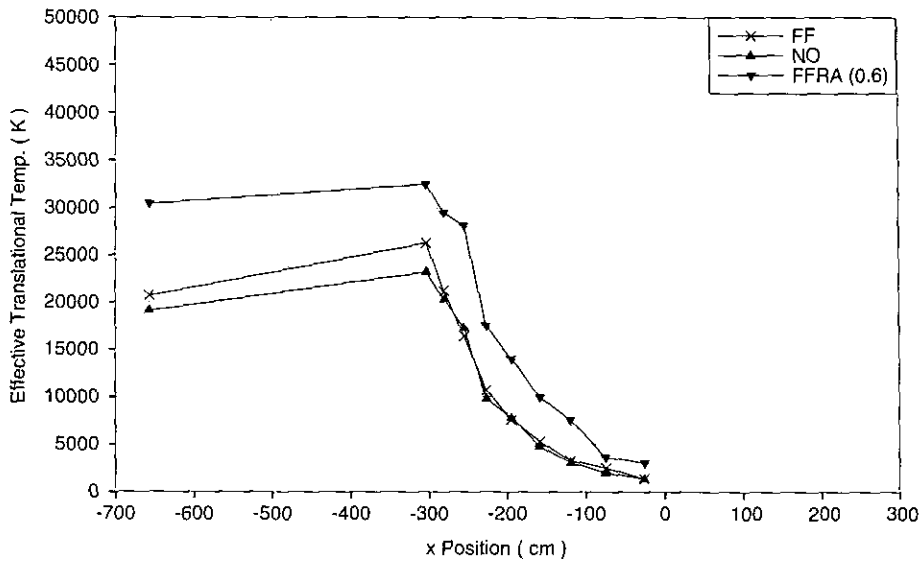

FIG. 15. Effective translational temperature along the axis of symmetry at 250 km: (▲) neutrals only, (×) full flow with full accommodation, (▼) full flow with a reduced (0.6) accommodation.

allowed for efficient modeling of the physics of the flow field. Nonphysical adaptations imposed by low level languages on current computers were reduced.

3. Aerothermochemistry-produced electron number density on the ram side was found to be significantly higher with a DSMC code as compared to full flow calculations.

4. The number density in the MBE growth area of the wake shield model is lower in the 250 and 500 km cases with the **E** field present than with it not present. The temperature is approximately the same. Consequently, the pressure is lower than would be predicted by a DSMC code.

5. The initial conditions of undisturbed equilibrium number density and energy state are critical in determining the near ram and near wake-flow fields.

6. Several flow field characteristics were bounded by this study, but not resolved in detail, particularly in the region of the near wake. The grid sizes imposed by physical computer limitations restricted the resolution of density gradients on the wake side. Specific areas of interest in a future study should be defined and investigated directly, such as a higher resolution near-wake structure for contamination concerns.

7. An accurate gas–surface interaction model (i.e., thermal accommodation, etc.) is essential in determining the near field conditions. The sensitivity of the solutions to the thermal accommodation is sufficient to render certain investigations invalid if the thermal accommodation is incorrectly modeled.

There are other areas for continued research using the modeling techniques described. Near ram side investigations can be accomplished in reentry flow problems. The **E** field gradients generated are such that the species distribution may alter the aerothermochemistry occurring behind the bow shock. Also, the parallel form of the code can be used to generate unsteady flow simulations on today's massively parallel machines. For example, a phasing-solution technique for an orbital or reentry flight through a varying atmosphere can yield time history studies in these conditions.

REFERENCES

1. T. Bartel, personal communication (Sandia National Laboratory, Albuquerque, NM), 1991.
2. G. A. Bird, *Molecular Gas Dynamics* (Clarendon Press, Oxford, 1976).
3. G. A. Bird, *Ann. Rev. Fluid Mech.* **10,** 11 (1978).
4. G. A. Bird, Monte Carlo simulation in an engineering context, in *12th International Symposium on Rarefied Gas Dynamics, 1981,* Vol. 74.
5. C. Borgnakke and P. S. Larsen, *J. Comput. Phys.* **18,** 405 (1975).
6. S. Chapman and T. G. Cowling, *The Mathematical Theory of Non-uniform Gases* (Cambridge Press, Cambridge, 1970).
7. A. S. Jursa, *Handbook of Geophysics and the Space Environment,* NTIS-ADA-167000 (1985).
8. C. R. Justiz and R. M. Sega, Full flow simulation of spacecraft in low earth orbit, in *22nd Fluid Dynamics, Plasma Dynamics, and Lasers Conference, Honolulu,* AIAA Paper 91-1500, 1991.
9. I. Katz, J. R. Lilley, G. A. Jongeward, M. J. Mandell, and T. T. Luu, *POLAR Code Validation,* GL-TR-89-0276 (1989).
10. W. Kinard, *LDEF Environ. Effects Newslett.* **II**(5), (1991).
11. E. C. Knox, F. G. Collins, and P. A. Liver, An engineering assessment of gas/surface interactions in free molecular aerodynamics, in *22nd Fluid Dynamics, Plasma Dynamics, and Lasers Conference, Honolulu,* AIAA Paper 91-1747.

12. NASA, *Space Station Freedom, Space Station External Contamination Control Requirements,* JSC 30426 (1986).
13. N.O.A.A., *U.S. Standard Atmosphere* (1976).
14. K. Rawer, *International Reference Ionosphere—IRI 79,* Report UAG-82 (1981).
15. R. M. Sega and A. Ignatiev, A space ultravacuum experiment: Application to material processing, in *Proc. Microgravity Sciences Symposium* (AIAA/IKA, Moscow, 1991).
16. R. E. Smith and G. S. West, *Space and Planetary Environment Criteria for Use in Space Vehicle Development,* 1982 Rev. Vol. 1 (1983).
17. W. G. Vincenti and C. H. Krueger, *Introduction to Physical Gas Dynamics* (Wiley, New York, 1987).